Life-Cycle Civil Engineering: Innovation, Theory and Practice – Chen, Ruan & Frangopol (Eds)

Early-warning system with fiber optic sensor networks and stability evaluation with model updating analysis

D.S. Xu & F.B. Zhu
School of Civil Engineering and Architecture, Wuhan University of Technology, Wuhan, P. R. China

ABSTRACT: Slope failure cause lots of casualties and assets loss. An early-warning system based on the fiber optic sensors and stability analysis with the Bayesian updating is proposed in this study. Fiber optic sensors has high accuracy and long-term stability, thus it could be employed for long-term measurement in slopes. In this study, a GFRP reinforced slope was used as an example to employ the slope health monitoring approach. The distributed BOTDA optical fiber sensors were successfully applied in quality evaluation and performance monitoring of an excavated slope. The random field modeling was incorporated in the model updating analysis to reduce the uncertainty of the soil parameters (e.g. cohesion c and friction angle φ). With the updating model, the slope stability could be verified with the field measurement data and further employed for stability evaluations, thus it could provide more accurate results for the health condition of the instrumented slope. This study could provide references for the slope stability evaluation system with smart sensing and on-line preformation evaluation.

1 INTRODUCTION

The slope stability is a very important issue during and after the construction of slope excavation (Chen et al. 2017; Jiang & Zhou 2017; Sun et al. 2018). It is of great significance to establish early-warning system with fiber optic sensor networks and stability analysis for safety. The fiber optic sensor networks were widely adopted as a newly advanced sensing technology to measure the full-distributed strain of slope for longtime (Xu & Yin 2016). However, slope stability analysis is related to many factors, such as field construction, rainfall and changes in groundwater levels. These external factors could affect the strength of the soil mass. Although soil parameters can be measured in field tests or in the laboratory, stability analysis using these soil parameters as mechanical parameters of numerical models may cause inaccurate results due to the spatial variability of soil, field observation data, and the disturbance of the construction process (Cao et al. 2016; Jiang et al. 2018; Li et al. 2014). Thus, accurately obtain the soil parameters is a key problem for stability analysis.

There is a need to quantify the soil parameters spatially due to the spatial variability of soil. To address this issue, random field element modeling (RFEM) implemented in finite element codes have been widely used in geotechnical engineering (Fenton & Griffiths 2008; Luo et al. 2018a). This method is usually used to study the effect of spatial variability of soil parameters on the response of geotechnical structures, for example the stability of soil dams and slopes (Griffiths & Fenton 2004; Wang et al. 2019), the structural response of supported excavations (Luo et al. 2018b; Montgomery and Boulanger 2016).

This paper aims to provide more accurate results for health condition of the instrumented slope. An early-warning system with fiber optic sensor networks and stability analysis with Bayesian updating was proposed to combine the measured data of fiber optic sensor with prior information and predict the stability of slope. The proposed method utilizes parametric modelling, random field modelling and Bayesian updating to reduce the uncertainty of the soil parameters (e.g. cohesion c and friction angle φ). The uncertainties of cohesion c and friction angle φ were analyzed with Bayesian updating method and applied in a field excavation study. The estimated results from the Bayesian method and field data were presented and discussed in details.

2 PRINCIPLE OF BOTDA

Brillouin Optic Time Domain Analysis (BOTDA) is a distributed sensing technology which realized by analyzing the backscattered signal generated inside the optical fibers. The working principle is shown

DOI:10.1201/9780429343292-135
https://doi.org/10.1201/9780429343292-135

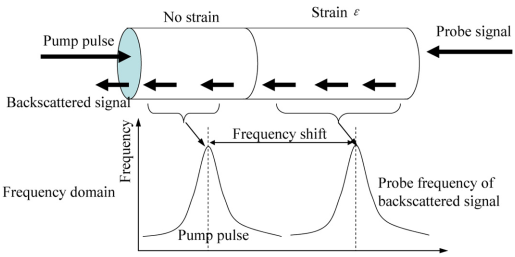

Figure 1. Measurement principle of the BOTDA.

in Figure 1. As indicated in the figure, when there is a laser light passing through the fiber, a small amount of scattered light was generated due to the non-homogeneities of the material. The frequency of scattering was changed due to the strain or temperature variations. The frequency shift ν_B is proportional to the acoustic velocity ν_a of scattering medium (Omnisens 2007), which can be expressed as follows:

$$\nu_B = \frac{2n\nu_a}{\lambda_0} \tag{1}$$

where n is the refraction index of fiber and λ_0 is the wavelength of the pump. The acoustic velocity ν_a is directly rated to the surrounding temperature and/or strain. The frequency shift has a linear relationship with the strain and temperature as follows (Horigchi et al. 1995):

$$\nu_B(\varepsilon) = \nu_B(0)[1 + C_\varepsilon \cdot \varepsilon] \tag{2}$$

$$\nu_B(T) = \nu_B(T_0)[1 + C_T \cdot (T - T_0)] \tag{3}$$

where $\nu(\varepsilon)$ and $\nu(T)$ represent Brillouin frequency shift at strain ε and temperature T, respectively. $\nu_B(0)$ and $\nu_B(T_0)$ are the reference frequencies. C_T and C_ε are constant coefficients related to temperature and strain, respectively.

3 FIELD INSTRUMENTATIONS

3.1 *Geology profile*

An excavated soil slope was adopted glass fiber reinforced polymer (GFRP) anchors to stabilize the slope. The responses of the GFRP anchor were measured by the distributed optical fibers during the excavation. The detailed information about this study and the distributed Brillouin optical time domain analysis was described by Xu & Yin (2016). In this study, CFRP anchors (EE9) was measured with the distributed optical fibers at different excavation stages. The detailed slope sections was shown in Figure 2. The slope is composed of four layers of soil. The upper soil layer of the slope was fill soil which sits above the completely decomposed granite (CDG) soil. The third soil layer was the highly decomposed granite (HDG) was

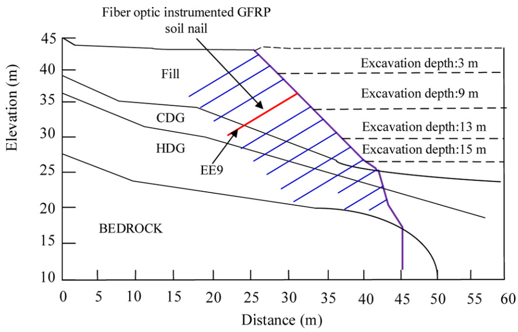

Figure 2. Cross section of the slope.

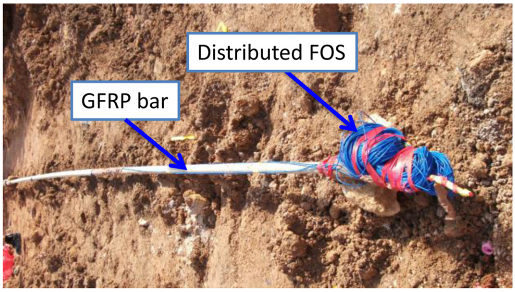

Figure 3. Photos of field instrumentation.

located above the bedrock which was the fourth soil layer. The slope excavation was carried put in four stages as described in Figure 2.

3.2 *Optical fibers for strain measurement*

Figure 3 shows the installation and protection for optical fiber sensors which were attached on the surface of the GFRP bar. The distributed optical fiber was installed with a "U" shape aluminum groove to protect fibers (Figure 2). The length of the used soil nail was 20m. Details of the installation information can be found from Xu et al. (2016). The unstrained optical fibers (around 2 m in length) were loosed at the end for better identifications. All the optical fibers heads were routed to the outside of the soil nails and subsequently terminated the slope crest. A separate set of temperature sensing cable was used to measure temperature. The fiber at the end of the soil nail also can be used as temperature sensors.

3.3 *Optical fibers for strain measurement*

The GFRP bar with distributed fiber optic sensor was installed in a drilling hole as shown in Figure 4. Briefly, the installation and monitoring process comprises five steps: (1) a hole was drilled with casing to prevent collapse; (2) GFRP bar was installed with distributed strain optical fiber sensors; (3) cement grouting inside of the hole; (4) curing after 7 days; (5) Data collections. The diameters of GFRP bar and drill-hole are

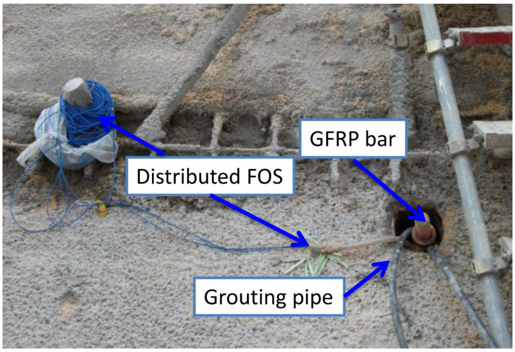

Figure 4. Installation of GFRP bar with fiber sensors.

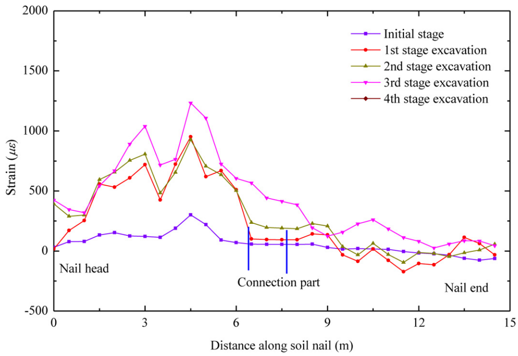

Figure 5. Distributed strain along soil nail EE9.

40mm and 150 mm, respectively. The GFRP soil nail is partially bonded in length 4.5m.

4 RESULTS ANALYSIS

4.1 *Distributed strain results*

The soil nail was deformed due to the excavation. Figure 5 depicted the results of GFRP soil nail EE9. Subsequent readings were taken during the four major excavations. The results show that the axial strain was around zero at the end of soil nail and then increased from the soil nail end to the maximum value. The position of maximum strain was at the middle section or sometimes near the slope surface.

4.2 *Numerical analysis*

A numerical model was established to be calibrated by on-site monitoring data. The monitoring data was the strain of GFRP anchor measured by the distributed optical fibers in four excavation stages. Figure 6 shows the finite element mesh and boundary conditions of soil slope.

Table 1 shows parameters of fill, CDG, HDG employed in this model. The hardening soil model

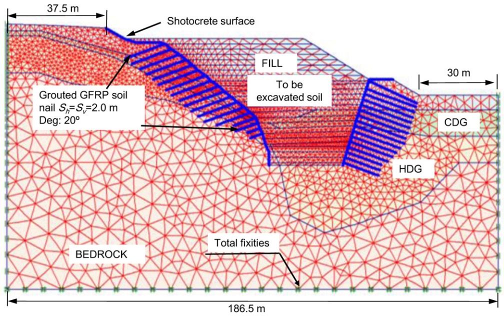

Figure 6. Finite element mesh and boundary conditions of soil slope.

Table 1. Soil parameters

Parameters		Fill	CDG	HDG	ROCK
Model	–	HS	HS	HS	MC
Unsaturated unit weight (kN/m^3)	γ_{unsat}	16.5	17	18	24
Saturated unit weight (kN/m^3)	γ_{sat}	17.5	18	19	25
Secant stiffness (MPa)	E^{ref}	60	200	600	5000
Tangent oedometer stiffness(MPa)	E^{ref}_{oed}	50	160	480	–
Unloading/ reloading stiffness (MPa)	E^{ref}_{ur}	800	1500	1500	–
Cohesion (kPa)	c	5	15	15	0
Friction angle (°)	φ	30	35	35	40
Dilatancy angle (°)	ψ	0	0	0	0
Poisson's ratio	V_{ur}	0.2	0.3	0.3	0.35
Lateral stress coefficient	K^{nc}_0	0.42	0.364	0.36	0.36

(HS model) was selected to represent the constitutive relationship of the three soils (e.g. fill soil, CDG soil and HDG soil). The bedrock was modeled as a Mohr-Coulomb model (MC model). The GFRP anchor reinforced system consists of a shotcrete surface, a nail head, GFRP anchors, couples, and centralizers. Thus, the system was divided into two parts which were modeled by elastic plate elements. The soil-anchor interaction was characterized by the interface reduction factor of R_{inter}. The detailed boundary conditions were presented in Figure 6. The excavation case was mainly divided into four stages which were 3 m, 9 m, 13 m, and 15 m.

Figure 7 shows the comparisons between the calculated results of the deterministic model with the measured results of the EE9 GFRP anchor at 8 points before and after the excavation stage. It can be seen that there is still a certain difference between the deterministic simulation results and the measured data. In

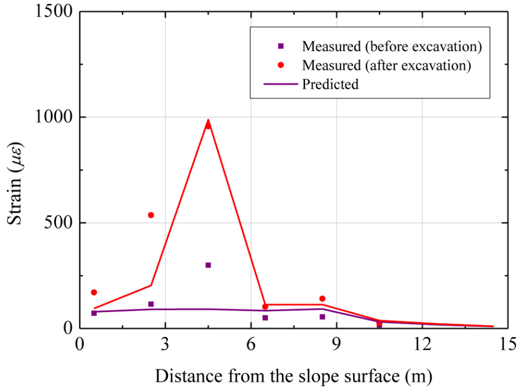

Figure 7. Comparison of the strains computed by numerical model and measured by the distributed optical fibers.

the first stage of excavation, although the average error between the numerical model results and the measured data is very small as 1.37 με, the peak value of the measured strain is at a position 4.5 m form the anchor head, and the peak value of the calculated strain is at 0 m. In addition, the strain increase of the numerical model is small in the last three excavation stages.

5 UPDATING ANALYSIS WITH RANDOM FIELD MODELLING

5.1 *Distributed strain results*

The stability of slope was related to the construction condition, rainfall, groundwater level change and shear strength of soil. The shear strength of soil is usually determined by cohesion c and friction angle φ. However, soil properties exhibits spatial variability due to the original soil properties and historical stress process (Wang & Cao 2013; Wang et al. 2016). In addition, in the Bayesian analysis of geotechnical engineering, the importance of determining soil properties was highlighted many times (Luo et al. 2018). The soil parameters in Bayesian updating are treated as random variables due to spatial variability, and their values have a very important relationship with their spatial location.

The scale of fluctuation, the correlation between two points and theoretical autocorrelation functions are important factors for describing the spatial variability of soil parameters by random field theory. The correlation between two locations (Salgado & Kim 2014; Wu et al. 2012; can be expressed as

$$\rho[T(x_i,y_i),T(x_j,y_j)] = \frac{COV(T(x_i,y_i),T(x_j,y_j))}{\sqrt{Var[T(x_i,y_i)]}\sqrt{Var[T(x_j,y_j)]}}$$

where $T(x_i, y_i)$ and $T(x_j, y_j)$ are the coordinates of two locations; Var and COV are the variance and covariance of soil parameters, respectively. The scale of fluctuation plays a key role in describing random field, which indicates the correlation between soil parameters and nearby soil area.

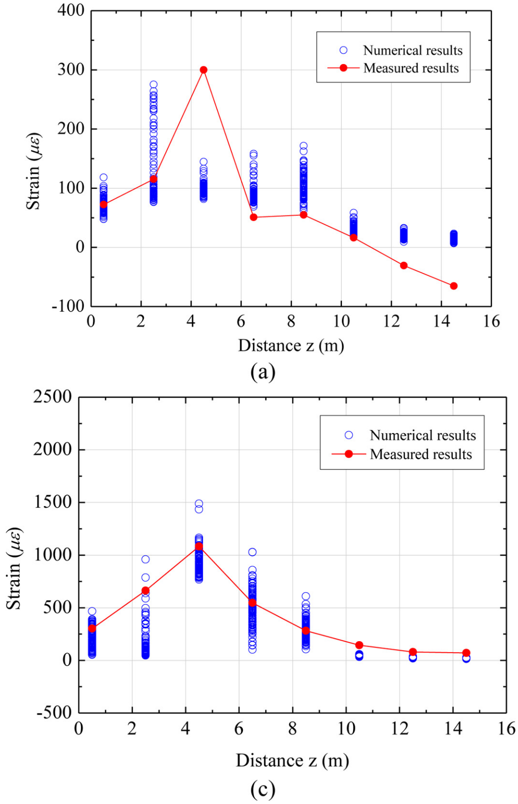

Figure 8. Comparison between numerical results of Bayesian distribution and measured data: (a) the numerical results in first excavation stages; (b) the numerical results in third excavation stages.

5.2 *Updating random variables by measurement data*

The Bayesian updating started from the first excavation stage and ended with the third stages. The parametric random field model is used as the model function of input parameters and the strain of EE9. In Bayesian updating, the first step is to determine the prior distribution of all random variables (i.e. c_1, c_2, c_3, φ_1, φ_2, φ_3, and φ_4), which were assumed to follow a lognormal distribution. The coefficients of variation (COV) of cohesion and friction angle are 0.3 and 0.2, respectively. Thus, the joint distribution of prior distribution was a multiplication of seven independent distributions.

Figure 8 shows the calculation results of EE9 at different monitoring points. The numerical calculation results varied with the uncertainly of soil parameters. However, with model updating, the calculation results of MCMCS were concentrated near the measured data.

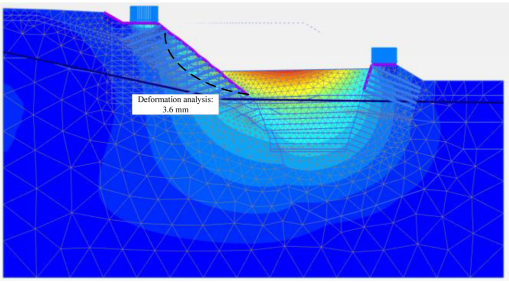

Figure 9. The computed critical slip surface of the instrumented slope.

It shows that Bayesian updating is helpful to improve prediction accuracy and guide construction with the increase of on-site monitoring data.

5.3 *Stability analysis*

The numerical analysis was conducted in accordance with the construction sequences in the field. The predicted critical slip surface by Plasticity calculation method is shown in Figure 10. The figure shows the most applicable failure mechanism of the soil nailed slope in the final stage and the deformation was 3.6 mm. Thus, the measured results can be combined with the numerical model for a better evaluation of the slope stability.

6 CONCLUSIONS

The distributed BOTDA optical fiber sensors were successfully applied in quality evaluation and performance monitoring of GFRP soil nails in an excavated slope. The field application of distributed BOTDA sensors and slope stability analysis with model updating was discussed in this study. The main conclusions are summarized as follows:

(1) The distributed BOTDA sensors were proved with a good accuracy for strain measurements. The BOTDA sensors were effective and efficient in field monitoring. Special efforts should be devoted to the fiber protection for sensor survival in the harsh environment.
(2) The uncertainty in geotechnical engineering has a significant influence on the stability analysis of slope. The random field modeling can effectively reduce the uncertainties in geotechnical engineering.
(3) A finite element model with Hardening Soil model was capable to model appropriately soil behavior of the stabilized slope under excavation conditions. The numerical analysis combined with model updating could improve accuracy of the prediction. The updating model can be used in the on-line preformation evaluation system and provide a more accuracy slope stability evaluation results for slopes.

REFERENCES

Cao, Z.J., Wang, Y., Li, D.Q., 2016. Site-specific characterization of soil properties using multiple measurements from different test procedures at different locations - a Bayesian sequential updating approach. *Eng. Geol.* 211: 150–161.

Chen, T., Deng, J.H., Sitar, N., Zheng, J., Liu, T.X., Liu, A., Zheng, L., 2017. Stability investigation and stabilization of a heavily fractured and loosened rock slope during construction of a strategic hydropower station in China. *Eng. Geol.* 22: 70–81.

Fenton, G. A., & Griffiths, D. V., 2008. *Risk assessment in geotechnical engineering.* Hoboken, NJ: John Wiley & Sons.

Grove, A.T. 1980. Geomorphic evolution of the Sahara and the Nile. In M.A.J. Williams & H. Faure (eds), *The Sahara and the Nile*: 21–35. Rotterdam: Balkema.

Griffiths DV, Fenton GA. Probabilistic slope stability analysis by finite elements. *J. Geotech. Geoenviron. Eng.* 2004; 130(5):507–18.

Horigchi, T., Shimizu, K., Kurashima, T., Tateda, M., and Koyamda, Y. (1995). “Development of a distributed sensing technique using Brillouin scattering.” Journal of Lightwave Technology, 13(7): 1296–1302.

Jappelli, R. & Marconi, N. 1997. Recommendations and prejudices in the realm of foundation engineering in Italy: A historical review. In Carlo Viggiani (ed.), *Geotechnical engineering for the preservation of monuments and historical sites*; *Proc. intern. symp., Napoli, 3–4 October 1996*. Rotterdam: Balkema.

Jiang, Q.H., Zhou, C.B., 2017. A rigorous solution for the stability of polyhedral rock blocks. *Comput. Geotech*. 90: 190–201.

Jiang, S.H., Papaioannou, I., Straub, D., 2018. Bayesian updating of slope reliability in spatially variable soils with in-situ measurements. *Eng. Geol*. 239: 310–320.

Johnson, H.L. 1965. Artistic development in autistic children. *Child Development* 65(1): 13–16.

Li, D.Q., Qi, X.H., Phoon, K.K., Zhang, L.M., Zhou, C.B., 2014. Effect of spatially variable shear strength parameters with linearly increasing mean trend on reliability of infinite slopes. *Struct. Saf.* 49: 45–55.

Luo, Z., Di, H.G., Kamalzare, M., Li, Y.X., 2018a. Effects of soil spatial variability on structural reliability assessment in excavations. *Underground Space*: 1–13.

Luo, Z., Li, T.X., Zhou, S.H., Di, H.G., 2018b. Effects of vertical spatial variability on supported excavations in sands considering multiple geotechnical and structural failure modes. *Comput. Geotech*. 95: 16–29.

Manual, U.’s., 2009. DITEST STA-R for Fiber Optic Distributed Temperature and Strain Analyzer. *Omnisens Corporation*. Morges, Switzerland.

Montgomery, J., Boulanger, R.W., 2016. Nonlinear deformation analyses of an embankment dam on a spatially variable liquefiable deposit. *Soil Dynamics and Earthquake Engineering*: 222–233

Polhill, R.M. 1982. *Crotalaria in Africa and Madagascar*. Rotterdam: Balkema.

Salgado, R., Kim, D., 2014. Reliability analysis and load and resistance factor design of slopes. *J. Geotech. Geoenviron*. 140 (1): 57–73.

Sun, Y., Jiang, Q.H., Yin, T., Zhou, C., 2018. A back-analysis method using an intelligent multi-objective optimization for predicting slope deformation induced by excavation. *Eng. Geol*. 239: 214–228.

Wang, Y., Cao, Z.J., 2013. Expanded reliability-based design of piles in spatially variable soil using efficient Monte Carlo simulations. *Soils Found*. 53: 820–834.

Wang, Y., Cao, Z.J., Li, D.Q., 2016. Bayesian perspective on geotechnical variability and site characterization. *Eng. Geol*. 203: 117–125.

Wu, S., Ou, C., Ching, J., Juang, C.H., 2012. Reliability-based design for basal heave stability of deep excavations in spatially varying soils. *J. Geotech. Geoenviron*. 138 (5): 594–603

Xu, D.S, Yin, J.H., 2016. Analysis of excavation induced stress distributions of GFRP anchors in a soil slope using distributed fiber optic sensors. *Eng. Geol*. 213: 55–63.